ACS APPLIED POLYMER MATERIALS

pubs.acs.org/acsapm
Article

Analysis of the Gas Transport Properties of the Polyoxymethylene Copolymer: Potential for Barrier Applications

Lorenzo Merlonghi, Perla Gavagni, Omar Atiq,* and Marco Giacinti Baschetti

Cite This: ACS Appl. Polym. Mater. 2026, 8, 2619−2631
Read Online

ACCESS | Metrics & More | Article Recommendations | Supporting Information

ABSTRACT: A comprehensive study of H_2, CO_2, O_2, and N_2 transport in a semicrystalline polyoxymethylene copolymer (POM-C) was conducted using the manometric time-lag method on 100 μm and 1 mm samples in the range −10 to 80 °C and 4−6 bar. Permeability, diffusivity, and solubility coefficients were determined, revealing CO_2 as the most permeable gas, followed by H_2, O_2, and N_2. The enhanced CO_2 permeability is attributed to favorable interactions with the ether groups in the polymer. POM-C showed excellent hydrogen barrier performance (0.44 Barrer at 20 °C and 0.04 Barrer at −10 °C) and good CO_2 barrier properties (1.6 Barrer at 20 °C and 0.215 Barrer at −10 °C). The results indicate the potential of POM-C for hydrogen and carbon dioxide storage and transport, suggesting that further investigation under higher-pressure conditions would be valuable to verify its suitability in such applications. The comparison between the two thicknesses indicates that hydrogen transport is minimally affected by the sample thermal history, whereas the other gases display moderate variations consistent with different crystallinity levels. POM-C also exhibits high CO_2/O_2 perm-selectivity (~34 at 20 °C), indicating potential for packaging applications requiring controlled oxygen ingress and moderate CO_2 exchange, particularly for moisture-sensitive products.

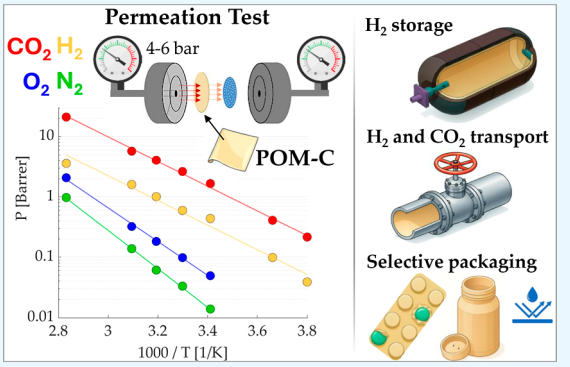

KEYWORDS: *polyoxymethylene, barrier polymers, gas permeation, gas diffusion, gas sorption, packaging, gas storage and transport*

1. INTRODUCTION

The study of gas transport in polymers has gained significant importance due to their broad use in separation membranes, selective packaging, and gas barrier liners for transport and storage.[1−4] In these applications, optimizing performance requires a detailed understanding of polymer properties and precise control over their microstructure. Semicrystalline polymers are distinguished among polymer classes by their coexistence of crystalline and amorphous phases, which impart transport properties unlike those of purely glassy or rubbery materials. In particular, the amount and distribution of crystalline regions, which are essentially impermeable to gas, result in a reduction in overall permeability.[5−7] This heterogeneous morphology not only allows fine-tuning of permeability and selectivity through control of microstructure and crystallinity but also enhances thermo-mechanical resistance, broadening their suitability for demanding applications.[8,9] Owing to these unique physicochemical features, semicrystalline polymers are increasingly employed in advanced technologies, particularly in gas barrier systems such as in packaging applications (i.e., Modified Atmosphere Packaging, MAP)[10] or gas liners in pipelines or vessels.[11]

1.1. Pure Gas High-Pressure Barrier

High-performance barrier polymers are critical in demanding applications, such as high-pressure hydrogen and carbon dioxide storage and transport. In hydrogen storage for fuel cell electric vehicle onboard systems, materials must combine excellent gas barrier properties with sufficient mechanical strength to withstand pressures up to 700 bar and repeated pressure fluctuations and temperature cycles associated with loading and withdrawal.[12,13] Within this framework, Type IV hydrogen storage tanks feature a semicrystalline polymer liner that forms the primary structure of the vessel, providing an effective barrier against gas permeation while substantially reducing weight compared to metallic designs.[1,14] In this framework, high-density polyethylene (HDPE) was initially employed for its high crystallinity (60−70%), which creates a significant tortuous path, slowing hydrogen diffusion. However, its relatively high hydrogen permeability and susceptibility to blistering under high pressure have revealed limitations in its long-term performance.[15,16] These drawbacks have led to the adoption of polyamide 6 (PA6) as the state-of-the-art polymer liner.[17] The strong intermolecular hydrogen

Received: October 14, 2025
Revised: January 30, 2026
Accepted: February 2, 2026
Published: February 10, 2026

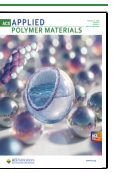

bonding in PA6 significantly enhances mechanical resistance, reduces gas permeation, and provides superior thermal stability—the latter reflects in its higher melting temperature (~230 °C vs ~130 °C for HDPE).[18,19] However, its hygroscopic nature still raises concerns about compromises in mechanical integrity and barrier performance due to relevant moisture uptake.[20−22] In the context of carbon capture, storage, and transport, the operating pressures are lower than in hydrogen storage (typically 100−400 bar).[23] Nevertheless, these applications require polymer materials that combine high chemical resistance with long-term stability to withstand the corrosive environment associated with supercritical CO_2 and resist plasticization. Fluoropolymers such as ETFE, PVF, and polyvinylidene fluoride (PVDF) are particularly well-suited to these conditions, as their robust C−F bonds provide exceptional chemical durability and sustained performance in the presence of supercritical CO_2 and associated impurities.[24] However, their widespread use is discouraged by costly synthesis processes and environmental concerns related to the persistence and toxicity of fluorinated compounds.[25]

1.2. Selective Barrier: Modified Atmosphere Packaging

Packaging and food packaging are other fields of application of very high importance for barrier polymers which even if less demanding in terms of operative conditions still pose challenges in the properties of materials. As an example, beyond high-pressure pure gas barriers, MAP needs to achieve a selectively permeable barrier tailored to the specific respiration rate of the packaged commodity.[26−30] The effectiveness of MAP, therefore, depends on the relative permeabilities of the primary gases involved—O_2, N_2, and CO_2—which regulate gas exchange, thereby controlling the internal atmosphere to preserve quality and extend shelf life:[26,27,31,32]

- Carbon dioxide inhibits microbial growth and slows respiration, making it particularly effective for meat, poultry, fish, and dairy. However, excessive CO_2 can cause off-flavors and package collapse due to absorption.
- Oxygen supports aerobic respiration in fresh produce and helps preserve the red color of raw meat, but high levels can accelerate oxidation and microbial spoilage. For low-respiring or processed foods, oxygen should be minimized.
- Nitrogen, an inert gas, displaces oxygen and prevents package collapse. It is commonly used in dry foods to reduce oxidation.[26,33,34]

Typical selectivity ratios are in the range of 3−6 for CO_2/O_2 and greater than 1 for O_2/N_2.[26,27,35,36] Polymers frequently employed in MAP include poly(vinyl chloride) (PVC), polyethylene terephthalate (PET), polypropylene (PP), and polyethylene, which are suitable for fresh products with relatively high respiration rates. For low-respiring commodities, materials with lower gas permeability, such as polyvinylidene chloride (PVDC) and PAs, are more appropriate.[26,27,34] Additionally, specialized materials such as ethylene vinyl alcohol (EVOH), PVDC, PVF, PVDF, and PET offer superior permeability control and environmental resilience.[26,37]

1.3. Polyoxymethylene

Polyoxymethylene (POM) has emerged as a highly promising material for a variety of applications. It combines exceptional mechanical, chemical, and tribological properties,[38,39] exhibiting the highest rigidity and strength among unreinforced engineering polymers and effectively bridging the performance gap between polymers and metals.[40] This combination of properties has enabled its use in precision engineering components such as gears, bearings, fasteners, and valves as well as in automotive parts, electrical connectors, and consumer appliances. Its intrinsic biocidal activity, derived from the controlled low release of formaldehyde, certified to remain well below established specific migration limit of 15 mg/kg,[41] may provide additional benefits in sterile packaging by actively reducing microbial contamination and enhancing hygiene and safety beyond those offered by conventional passive barriers.[42] POM typically exhibits a crystallinity between 50 and 60% and melts at temperatures ranging from 160 to 170 °C,[40,43,44] placing its thermo-mechanical resistance comfortably between those of HDPE and PA6.[18] Its dense amorphous phase, with a density of 1.23 g/cm^3—higher than that of PA6—suggests strong potential as an effective barrier,[17] while its low water uptake (0.2−0.8 wt %[45]) offer resistance to swelling and plasticization that could otherwise degrade performance over time. Furthermore, POM demonstrates excellent chemical stability, resisting a wide variety of substances, including supercritical CO_2.[46] Its moderate cost and absence of fluorine offer additional environmental benefits, simplifying recycling and enhancing sustainability relative to many fluoropolymer alternatives.[47,48] Despite these advantages, the homopolymer form (POM-H) has limitations, particularly UV-induced degradation via a chain "unzipping" mechanism, which can lead to embrittlement and mechanical failure over time.[49] The copolymer polyoxymethylene copolymer (POM-C) incorporates small amounts of ethylene oxide units along the chain. This slightly disrupts molecular order and reduces crystallinity, yet in doing so, it stabilizes the polymer by halting the unzipping process, enhancing resistance to UV radiation, oxidation, and harsh environmental conditions while largely preserving the mechanical integrity of the homopolymer. These features naturally favor the use of POM-C in applications where long-term stability is critical, compared with the homopolymer.[50]

Although POM-C exhibits a range of promising characteristics, its gas transport properties have remained insufficiently characterized. Existing studies primarily report few permeability values at ambient temperature for gases such as oxygen, nitrogen, and carbon dioxide,[37,43,51] with little to no information on temperature dependence, the influence of processing conditions (e.g., thickness), and the separate contributions of diffusivity and solubility. Moreover, to the best of the authors' knowledge, no data are currently available on hydrogen permeation. This lack of information hinders a comprehensive evaluation of gas transport behavior in POM-C and underscores the need for targeted experimental investigation. Accordingly, this study aims to address this gap by systematically examining the permeation, sorption, and diffusion of hydrogen, carbon dioxide, oxygen, and nitrogen in POM-C at pressures between 4 and 6 bar and temperatures ranging from −10 to 80 °C. Two samples of different thicknesses (a 110 μm film and a 1 mm slab), each reflecting unique processing histories and morphologies, were examined to assess the impact of processing conditions on transport properties. This study aims to provide a comprehensive understanding of the gas transport behavior of POM-C, positioning its performance within the broader context of semicrystalline polymers and evaluating its potential as an alternative material for gas barrier and packaging applications.

https://doi.org/10.1021/acsapm.5c03855
ACS Appl. Polym. Mater. 2026, 8, 2619−2631

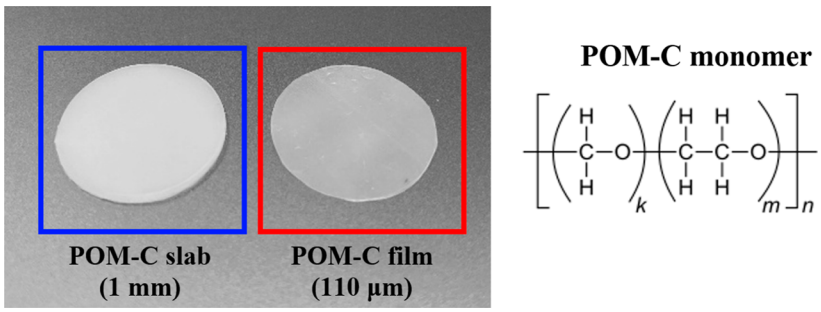

Figure 1. Images of the POM-C slab (1 mm) and the hot-melted, pressed film (110 μm), along with the chemical structure of the POM-C monomer.

2. THEORETICAL BACKGROUND

The extent to which a material permits or impedes gas transport can be quantified by its permeability, defined as the ratio of the gas flux to the pressure gradient across the material thickness. More in detail, when a pressure difference Δp is applied across a material sheet of thickness L, a constant flux per unit surface, J_s, is established at the steady state, leading to the following expression:

$$J_s = P\frac{\Delta p}{L} \tag{1}$$

where P is the permeability coefficient or simply the gas permeability of the membrane. In the context of dense polymeric materials, permeation follows the solution-diffusion mechanism;[52] consequently, the permeability can be expressed as the product of the sorption and diffusion coefficients:

$$P = S{\cdot}D \tag{2}$$

Indeed, while eq 1 describes the steady state condition, the transient process strictly depends on the diffusion coefficient and can be described through the analytical solution of the local mass transport equation with appropriate boundary conditions.[53] In this framework, for the specific case in which the upstream interface is kept at a constant concentration C_u while the downstream concentration and the initial concentration in the overall material domain are equal to zero, the number of permeated moles per unit area, Q_t, in the time interval of $(0; t)$ can be expressed as

$$Q_t = \frac{C_u D}{L}t - \frac{LC_u}{6} - \frac{2}{\pi^2}\sum_{n=1}^{\infty}\frac{-1^n}{n^2}\exp\left(-\frac{Dn^2\pi^2}{L^2}t\right) \tag{3}$$

As time goes to infinity, a steady state is attained, and the expression simplifies to

$$Q_{t,s} = \frac{C_u D}{L}t - \frac{LC_u}{6} \tag{4}$$

From the slope of eq 4, also defined as the steady state molar flux ($J_s = dQ_{t,s}/dt$), it is possible to calculate the permeability coefficient P according to eq 5, while the diffusion coefficient, D, can be extracted from the Q_t-axis intercept through eq 6:[54]

$$P = \frac{dQ_{t,s}}{dt}\frac{L}{\Delta p} \tag{5}$$

$$D = \frac{L^2}{6\tau} \tag{6}$$

where τ represents the time lag.

Finally, the solubility coefficient S can be estimated either from the ratio of P and D (eq 2) or, alternatively, from eq 4 using its definition as the ratio of the penetrant concentration in the membrane, C_u, to its partial pressure in the gas phase (p_u), as follows:

$$C_u = -\frac{6Q_{t,s}|_{t=0}}{L} \tag{7}$$

$$S = \frac{C_u}{p_u} \tag{8}$$

The temperature dependence of the permeability, diffusivity, and solubility coefficients is typically expressed through Arrhenius equations:[55]

$$P = P_0\exp\left(-\frac{E_P}{RT}\right) \tag{9}$$

$$D = D_0\exp\left(-\frac{E_D}{RT}\right) \tag{10}$$

$$S = S_0\exp\left(-\frac{\Delta H_S}{RT}\right) \tag{11}$$

where R is the gas constant, P_0, D_0, and S_0 are the pre-exponential factors corresponding to a temperature approaching infinity. Term E_P represents the activation energy for the permeation which is the sum of the activation energy of the diffusion, E_D, and the enthalpy of sorption, ΔH_S. While the diffusivity of gases in polymers always increase with temperature, as reflected by positive E_D values, the solubility can increase or decrease with temperature, depending on the balance between condensation and mixing enthalpies.[56] For instance, while the solubility of larger, highly condensable gases like carbon dioxide decreases with rising temperature, small, incondensable gases such as hydrogen have been reported to exhibit positive ΔH_S values, indicating an increase in solubility with temperature.[55]

The permeability of a material is the key parameter in controlling gas transport. In compressed gas storage, minimizing P is essential to reduce leakage to the atmosphere, which requires leveraging both solubility (S) and diffusivity (D). In MAP applications[26] and gas separation processes,[57−60] instead, the goal extends to controlling the relative transport of different gases—enhancing the passage of some while restricting others. Therefore, the focus shifts to optimizing the perm-selectivity, $\alpha_{P,ij}$, defined as the ratio of the permeability of the more permeable gas i to that of the less permeable gas j:

https://doi.org/10.1021/acsapm.5c03855
ACS Appl. Polym. Mater. 2026, 8, 2619−2631

$$\alpha_{P,ij} = \frac{P_i}{P_j} = \frac{D_i}{D_j}\frac{S_i}{S_j} = \alpha_{D,ij}\cdot\alpha_{S,ij} \quad (12)$$

Once again, it is possible to distinguish the solubility selectivity $\alpha_{S,ij}$ and diffusivity selectivity $\alpha_{D,ij}$. Eq 12 is commonly referred to as the ideal selectivity, as it is based on pure-gas permeability measurements and therefore may not accurately represent the real separation performance of a given membrane under mixed-gas conditions. Nevertheless, it is typically used as a reference parameter to compare the behavior of different materials in preliminary assessments, such as the one presented in this study.

3. MATERIALS AND METHODS

3.1. Materials

POM-C was supplied by Alt-Intech (Alt-Technischer Handel GmbH) as a 1 mm thick slab. A thin film with a thickness typical of packaging applications (110 μm) was produced from the same material by mechanically reducing the slab into small fragments, hot-melting, and pressing the resulting pieces at 200 °C (T_m = 168 °C) in a Carver Model C laboratory press (15 tons, 15.2 × 15.2 cm platens). Both the as-received slab and the processed film were characterized to evaluate the effect of processing-induced morphology and thickness on gas transport properties. Images of the two circular specimens are shown in Figure 1. The chemical structure of the POM-C monomer, also reported in Figure 1, consists of methylene oxide (k) and ethylene oxide (m) repeating units. POM-C, therefore, spans the compositional range between the polyoxymethylene homopolymer (POM-H, m = 0) and poly(ethylene oxide) (PEO, k = 0). However, with a typical m/k molar ratio of approximately 2%, POM-C is structurally much closer to POM-H.

3.2. Density and Crystallinity

The mass degree of crystallinity X_c and the melting temperature T_m of both samples were measured using a differential scanning calorimeter (DSC) equipment (TA INSTRUMENTS, DSC Q10). The analysis was conducted according to the following procedure: a sample of about 20 mg was cut in the form of a circular disk with diameter equal to 5 mm and placed in the sample holder, to be tested under a nitrogen flow rate of 20 cm^3/min with a heating ramp of 10 °C/min, going from −50 to 200 °C. During the heating, the heat flux absorbed by the material was measured, allowing for the estimate of the melting temperature and the heat of melting, ΔH_m. The mass crystallinity was finally evaluated through the following equation:[55]

$$X_c = \frac{\Delta H_m}{\Delta H_c} \quad (13)$$

where the heat of melting of the fully crystalline material, ΔH_c, was taken equal to 317.93 J/g.[43]

The density of the semicrystalline materials ρ was measured at ambient conditions (1 bar, 20 °C) through Archimedes' principle by using reagent-grade acetone (≥99.5%, Sigma-Aldrich) as the immersion fluid.[61]

3.3. Permeation Tests

The gas transport properties of POM-C samples were characterized by single-gas permeation tests, using high-purity gases (≥99.9%, CO_2, H_2, O_2, N_2) purchased from Fluido Tecnica S.A.S. Measurements on the film were performed in the temperature range of −10−80 °C for H_2 and CO_2 and 20−80 °C for O_2 and N_2. Due to time constraints, only a limited set of tests were carried out on the slab, in the range of 30−50 °C, to assess whether the different processing conditions (and the resulting crystallinity differences) affect the transport properties of the gases investigated. The fixed-volume manometric permeation apparatus, already described in a previous work,[17] is housed in a compressor-cooled incubator (Memmert ICP110), allowing measurements down to −12 °C, and comprises two calibrated volumes separated by a permeation cell. The upstream volume, connected to the gas reservoir, is loaded with gas at the desired pressure, while the downstream volume is kept in static vacuum and connected to a low-pressure manometer, used to monitor the increase of pressure corresponding to the permeating number of moles per unit area. A gastight contact between the upstream side of the cell and the sample is ensured by a rubbery O-ring, while the downstream side of the cell is supported by a sintered filter (1.5 cm diameter) with negligible resistance to gas flow, which provides mechanical support against the upstream pressure. Both the upstream and downstream sides are connected to the Edwards Rotary Pump RV5 for vacuum generation and the purge line, which is equipped with a Bunsen burner to combust excess flammable gases after each experiment. The upstream pressure is measured using a high-pressure manometer (DRUCK Leicester PTX1400 EX-0129), with an accuracy of 0.01 bar and a range of 0−6 bar, while the downstream pressure is monitored with a low-pressure capacitive manometer (Setra Model 730), featuring an accuracy of 0.01 mbar and a range of 0−100 mbar. Circular specimens (2.5 cm diameter) obtained from the pristine slab and the film (shown in Figure 1) were mounted in the permeation cell. Before testing, the whole system was subjected to dynamic vacuum conditions for varying durations, up to 5 days for the slab, to remove any residual adsorbed gases. A leak test was then performed by monitoring the downstream pressure increase in static vacuum to ensure that the system was leak-proof and that the sample did not release any residual substance. The test began by filling the upstream side with the desired gas up to the experimental pressure while the downstream pressure was recorded over time. Since the upstream volume is significantly larger than the downstream volume, the upstream pressure remained practically constant throughout the test. On the other hand, after the time lag has elapsed, the downstream pressure began to increase steadily, but it remained negligible (several orders of magnitude lower) with respect to the upstream pressure, so that eqs 3−5 were applicable. Due to the low-pressure regime, ideal gas conditions hold true, allowing the conversion of the downstream pressure p_d to the number of permeating moles per unit area Q_t at a given time through the ideal gas law:

$$Q_t = \frac{p_d V_d}{ART} \quad (14)$$

where V_d is the downstream volume, A is the permeation area, which is taken equal to the area of the sintered filter, R is the ideal gas constant, and T is the temperature. Then, the permeability, diffusivity, and solubility coefficients were calculated by using eqs 5, 6, and 2, respectively. Hydrogen permeation measurements on two POM-C film specimens at 30 °C were used to estimate the relative standard deviations of the measured properties, denoted as $\varepsilon_r(P)$, $\varepsilon_r(D)$, and $\varepsilon_r(S)$, which resulted to be rather limited and in the order of 1%, 6%, and 7%, respectively, for permeability diffusivity, and solubility. These values were subsequently used as reference uncertainties for all tests performed at different temperatures and with other gases.

4. RESULTS AND DISCUSSION

4.1. Material Characterization

Figure 2 shows the DSC curve of POM-C samples, illustrating the normalized heat absorbed per unit time and mass as a function of temperature. The resulting measured crystallinities and the density are summarized in Table 1 and compared to the literature reference, showing substantial agreement.

The DSC results indicate that the thin films melt at a slightly lower temperature ($T_m \approx 164$ °C) with a higher, sharper peak, consistent with a uniform crystal population. In contrast, the thick slab shows a broader, lower intensity melting peak centered at $T_m \approx 168$ °C, indicative of a wider distribution of thicker crystals. This behavior reflects more developed crystallization in the bulk, whereas the film is likely dominated by surface-driven crystallization due to its thin geometry and faster cooling. Ultimately, the higher heat of fusion of the slab

https://doi.org/10.1021/acsapm.5c03855
ACS Appl. Polym. Mater. 2026, 8, 2619−2631

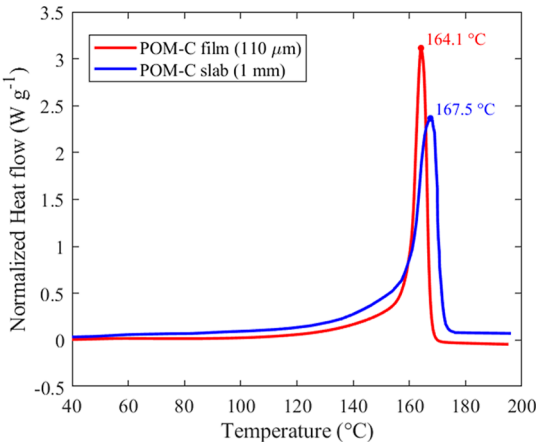

Figure 2. DSC curves of POM-C samples: film (red) and slab (blue).

Table 1. Properties of POM-C in Film and Slab Forms Compared with Literature Data

	this work (T.W.)		
property	film	slab	literature data
melting temperature (°C)	164.1	167.5	165 (Jiao et al.[44])
melting enthalpy (J/g)	144.3	157.9	
mass crystallinity (%)	45.4	50	50 (Kongkhlang et al.[43]) 51 (Jiao et al.[44])
density (g/cm^3)		1.41	1.41−1.51 (Fink[51])

compared to the film denote a slightly greater overall mass degree of crystallinity.

4.2. Permeation Test Results

The permeability, diffusivity, and solubility coefficients for the film and slab samples at all investigated temperatures following the procedure described in Section 3.3 are summarized in Table 2. For illustration, representative experimental permeation curves for the slab sample at 30, 40, and 50 °C are displayed in Figure S1 of the Supporting Information. The latter provides clear insights into the transport behavior of the investigated gases. Hydrogen exhibited a very short time lag (less than 2 h); the slab thickness allows a careful and more precise detection of the time lag for such fast gases, especially at higher temperatures. In contrast, the other gases required significantly longer times to reach a steady state (approximately 10−30 h), making these measurements considerably more time-consuming. A clear temperature dependence is evident for all gases, reflecting the rate of diffusion through the membrane.

The observed trend of permeability followed the order $P_{CO_2} > P_{H_2} > P_{O_2} > P_{N_2}$, which aligns with typical behavior reported for these classes of materials.[58,62,63] Carbon dioxide exhibits a permeability approximately four times higher than that of hydrogen, primarily due to its sorption coefficient, which is nearly 2 orders of magnitude greater. Oxygen and nitrogen exhibit permeabilities about 1 order of magnitude lower than that of hydrogen, with oxygen permeability always higher than that of nitrogen.

Notably, the hydrogen permeability values are nearly identical for the film and the slab. Differences in crystallinity affect the diffusion path length of the molecule (tortuosity) compared to that of its free path. However, since hydrogen has

Table 2. Permeability, Solubility, and Diffusivity Coefficients of CO_2, H_2, O_2, and N_2 in POM-C for the 100 μm Film and the 1 mm Slab in the Pressure Range of 4−6 bar[a]

	T [°C]	P [Barrer]		D [10^7 cm^2/s]		S [10^3 cm$^3_{STP}$/cm^3 cm Hg]	
gas		film	slab	film	slab	film	slab
CO_2	−10	0.215		0.0084		25.53	
	0	0.410		0.0229		17.90	
	20	1.66		0.14		12.01	
	30	2.63	1.60	0.22	0.12	11.84	13.36
	40	4.06	2.20	0.51	0.23	8.03	9.58
	50	5.73	3.51	0.75	0.44	7.71	7.71
	80	21.08		4.16		5.06	
H_2	−10	0.04		0.549		0.07	
	0	0.10		1.15		0.10	
	20	0.44		3.00		0.15	
	30	0.60	0.52	3.70	3.40	0.16	0.15
	40	1.01	0.84	5.67	4.90	0.18	0.17
	50	1.60	1.38	6.45	7.20	0.25	0.19
	80	3.6		11		0.33	
O_2	20	0.049		0.134		0.37	
	30	0.098	0.08	0.296	0.20	0.33	0.40
	40	0.182	0.113	0.572	0.36	0.32	0.36
	50	0.322	0.23	1.06	0.68	0.31	0.34
	80	2.08		7.06		0.29	
N_2	20	0.014		0.06		0.23	
	30	0.033	0.07	0.15	0.17	0.22	0.43
	40	0.061	0.12	0.30	0.30	0.20	0.39
	50	0.138	0.21	0.88	0.59	0.16	0.36
	80	0.975		7.32		0.13	

[a]The relative errors are $\varepsilon_r(P) = 1\%$, $\varepsilon_r(D) = 6\%$, and $\varepsilon_r(S) = 7\%$.

https://doi.org/10.1021/acsapm.5c03855
ACS Appl. Polym. Mater. 2026, 8, 2619−2631

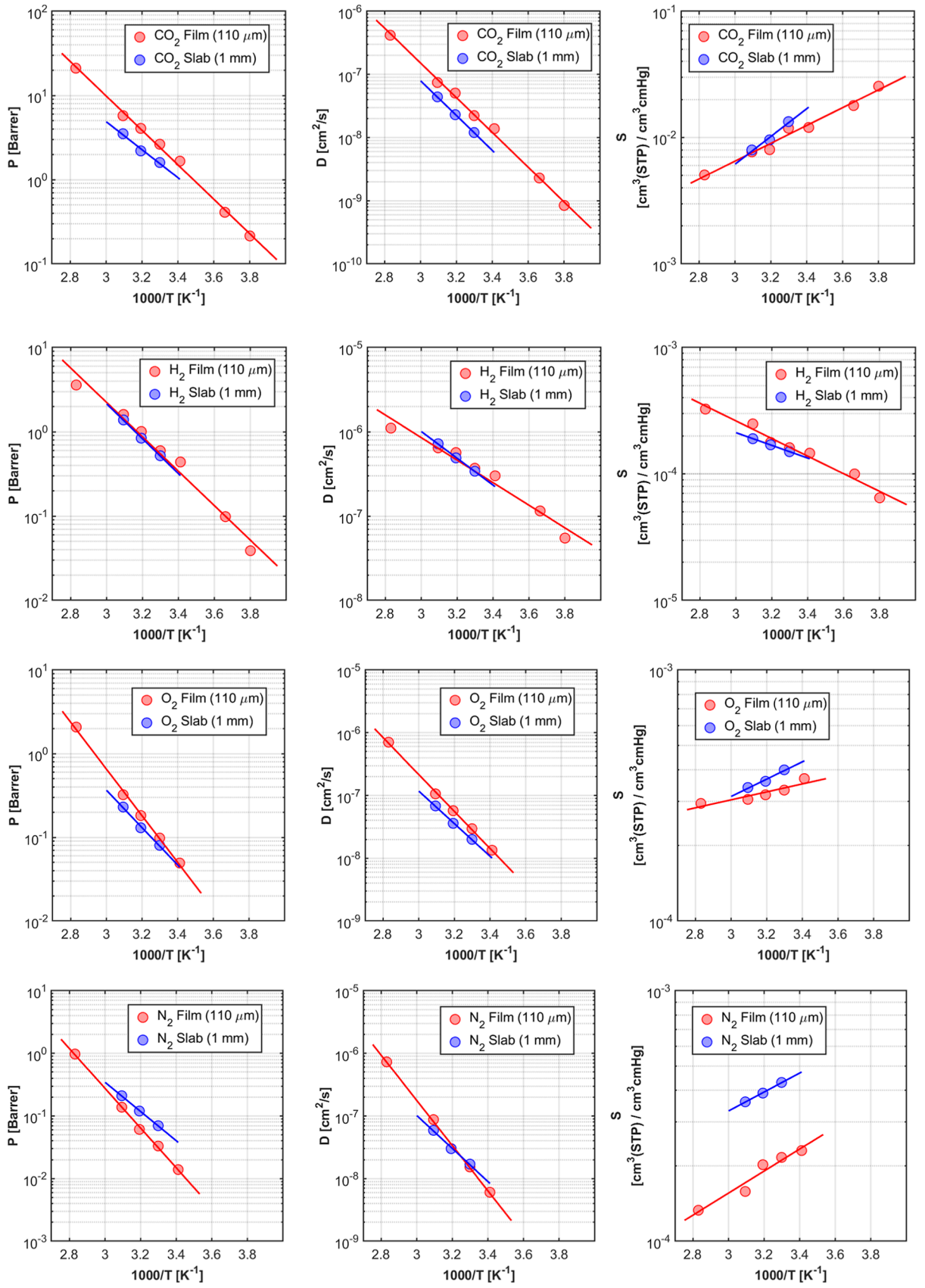

Figure 3. Temperature dependence of permeability, diffusivity, and solubility coefficients for CO_2, H_2, O_2, and N_2 in POM-C. Experimental measurements for the film (110 μm, red dots) and the slab (1 mm, blue dots). Arrhenius fitting lines are obtained using eqs 9−11 (solid lines); parameters are reported in Table 3.

https://doi.org/10.1021/acsapm.5c03855
ACS Appl. Polym. Mater. 2026, 8, 2619−2631

Table 3. Arrhenius Parameters for CO_2, H_2, O_2, and N_2 in POM-C, Obtained Using eqs 9−11 on Table 2 Data (Film and Slab)

	P_0 [10^{-6} Barrer]		E_p [kJ/mol]		D_0 [cm^2/s]		E_d [kJ/mol]		S_0 [$10^6\ cm^3_{STP}/cm^3\ cm\ Hg$]		ΔH_s [kJ/mol]	
	film	slab	film	slab	film	slab	film	slab	film	slab	film	slab
CO_2	13.76	0.49	39.20	31.92	27.90	15.51	52.73	52.89	49.24	3.09	−13.53	−21.04
H_2	3.03	3.61	39.13	39.73	0.0089	0.06	25.65	30.54	32,557	6852	13.35	9.63
O_2	158.9	1.98	53.5	42.95	154.1	7.51	56.49	49.80	101.4	28.54	−3.04	−6.64
N_2	928.3	3.52	60.78	44.72	12,422	8.72	69.20	50.61	7.44	24.26	−8.42	−7.24

very high mobility, the slightly greater crystallinity of the slab (≈50% vs ≈45%) does not significantly affect the diffusivity. As a result, hydrogen permeability is practically independent of sample thickness, meaning that thin-film measurements can reliably represent hydrogen transport in thicker liners, i.e., those required for high-pressure storage applications. On the other hand, for the other gases, permeability differences between the film and the slab are more evident, particularly for CO_2. Larger molecules already diffuse slowly through the amorphous phase; therefore, their transport is more strongly affected by the tortuosity introduced by crystalline regions, making the impact of crystallinity more pronounced. The higher crystallinity of the slab, therefore, leads to a reduction of the diffusivity and ultimately permeability of CO_2 and O_2 compared to the film. The opposite trend observed for N_2 represents an outlier and is likely attributable to experimental variability or incomplete degassing during slab equilibration, which may result in a marginal overestimation of the permeability. The pronounced difference in solubility observed for this gas further corroborates this hypothesis. Despite this uncertainty, the overall observed differences are modest, indicating that the transport properties of the two samples are similar, notwithstanding differences in their processing histories. A more detailed analysis of these results will be provided in later, when the experimental values for POM-C film are compared with those of other polymers.

Permeability increased with temperature for all gases primarily due to enhanced diffusivity. Solubility decreased with temperature for CO_2, O_2, and N_2, while hydrogen showed the expected opposite trend.[17,64] A more detailed analysis of the temperature dependence of permeability, diffusivity, and solubility coefficients is presented in Figure 3, where the experimental data were fitted using Arrhenius relationships (eqs 9−11) to extract pre-exponential factors and activation parameters for each gas in both types of samples.

The Arrhenius fits confirm the expected temperature dependence with diffusivity being the dominant factor, governing the increase in permeability with temperature. The quality of the fit is excellent for permeability and diffusivity, with a minimum R^2 value of 0.98. For the sorption coefficient, however, the fit quality is slightly lower because the calculation of S from the ratio of P and D amplifies experimental errors; nevertheless, the R^2 coefficient remains at least 0.85. The fitted parameters are reported in Table 3.

The comparison of transport behavior among gases and between the two samples relies primarily on the activation energies since the pre-exponential factors are intrinsically subject to large variability. In this context, carbon dioxide and hydrogen exhibit comparable activation energies for permeation, both lower than those of oxygen and nitrogen. However, the contributions of diffusion and sorption to E_p differ significantly among the two gases. The high activation energy of diffusion of CO_2 is compensated by a strongly negative enthalpy of sorption, which lowers the overall activation energy of permeation. In contrast, for hydrogen, the temperature dependence of permeability is mainly driven by the low activation energy for diffusion since its enthalpy of sorption is positive. This positive value reflects the comparatively minor contribution of endothermic condensation to the overall sorption enthalpy, relative to the other gases.[64] Comparing the two samples, the film exhibits higher activation energies of permeation than the slab (except for H_2), indicating more thermally activated transport. This is consistent with the slab having a slightly higher degree of crystallinity, which reduces the temperature sensitivity of permeation. Hydrogen is the exception, as its small size makes its transport less affected by microstructural differences, as already stated.

4.3. Gas Barrier Performance

This section presents a comparative analysis of gas transport in POM-C (film) and other barrier polymers to contextualize POM-C's performance within the broader landscape of polymers with permeability plotted against molecular kinetic diameter (d_k) in Figure 4. Subsequent figures separate permeability into diffusion and sorption contributions, with diffusivity plotted against the kinetic diameter (Figure 5) and sorption against the gas critical temperature (Figure 6). This breakdown is commonly used in literature to compare the value of these quantities for different gases while underlining their different character, mainly kinetic for diffusivity and thermodynamic for solubility.[65,66] The charts provide further insight into the transport mechanisms, showing how trends across different materials can reveal insights into the influence of their structural and chemical variations on gas transport behavior.

The results obtained in this work for the POM-C film are in the same order of the literature values for a general POM,[55] confirming its low permeability across all gases. The polymer exhibits excellent hydrogen barrier performance comparable to established engineering polymers such as PVDF and PA6. While EVOH remains the polymer with the highest intrinsic barrier properties, its sensitivity to moisture restricts direct structural use, so it is typically employed in multilayer systems.[71] POM-C combines good barrier performance with low water uptake, making it a promising alternative for high-pressure hydrogen storage, though its structural integrity under high-pressure conditions should be carefully assessed.

Regarding carbon dioxide, POM-C exhibits moderate barrier performance, with permeability values significantly lower than those of FEP, ETFE, and PTFE. This combined with its excellent compatibility with dry, humid, and supercritical CO_2 as well as with carbonic acid highlights its potentiality for carbon capture, storage, and transport systems.[46,72−74] Furthermore, its nonfluorinated backbone offers a more sustainable alternative, reducing environmental impact while enhancing applicability in mechanical support components and moving parts such as gears, rollers, guides, low-pressure valves,

https://doi.org/10.1021/acsapm.5c03855
ACS Appl. Polym. Mater. 2026, 8, 2619−2631

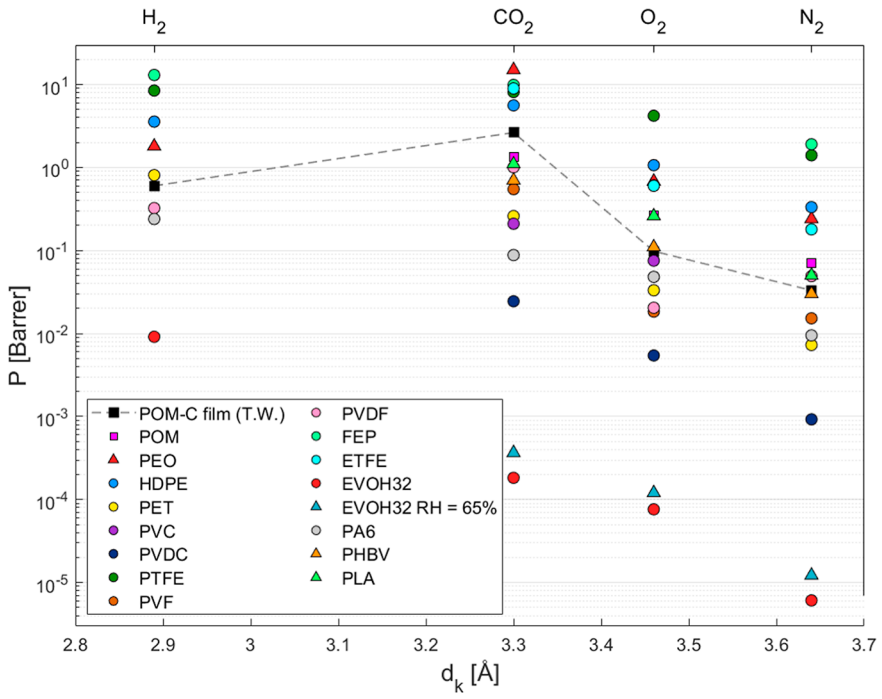

Figure 4. Permeability coefficients of gases in the POM-C film (this work T.W.) vs kinetic diameter at 30 °C; literature data of other polymers: generic POM,[55] PEO,[58] HDPE,[55,67] PET,[55,68] PVC,[37] PVDC,[37] PFTE,[23] PVF,[23] PVDF,[24,37] FEP,[24,37] ETFE,[24,37] EVOH32,[69] PA6,[17,37] PHBV s,[66] and PLA.[70]

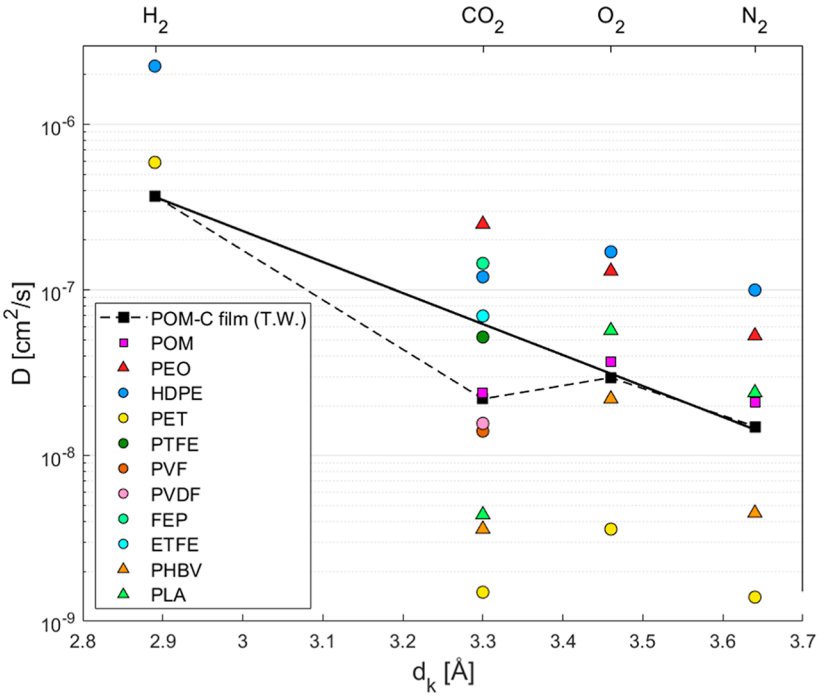

Figure 5. Diffusion coefficients of gases in the POM-C film (this work T.W.) vs kinetic diameter at 30 °C. The continuous fitting line refers to the data set without CO_2, according to eq 15; literature data of other polymers generic POM,[55] PEO,[58] HDPE,[55,67] PET,[55,68] PFTE,[24,37] PVF,[23] PVDF,[24,37] FEP,[23] ETFE,[24,37] PHBV,[66] and PLA.[70]

and actuation mechanisms, thanks to its excellent wear resistance.[40] Across the other gases (O_2 and N_2), POM-C maintains good barrier properties, reinforcing its versatility in multi-gas environments. Its balanced permeability profile, combined with humidity resistance and mechanical robustness, supports its use in advanced barrier systems.

Notably, the CO_2 permeability lies above the general pattern observed for the other gases, indicating that its transport behavior deviates from the expected size-dependent trend and suggesting that thermodynamic interactions may play a significant role. This behavior will be examined further by analyzing separately the contributions of diffusivity (Figure 5) and solubility (Figure 6) trends.

https://doi.org/10.1021/acsapm.5c03855
ACS Appl. Polym. Mater. 2026, 8, 2619−2631

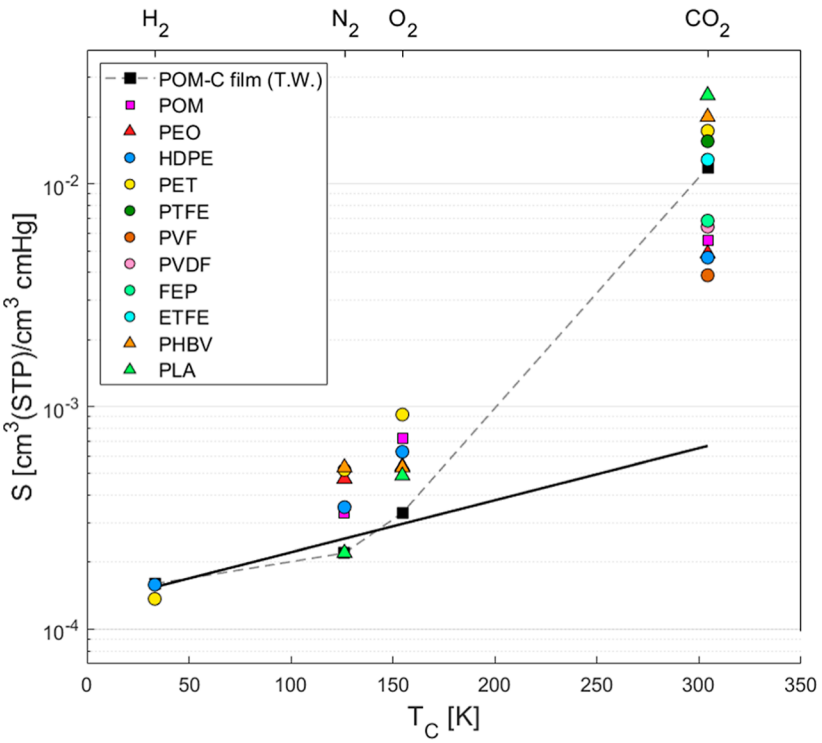

Figure 6. Solubility coefficients of gases in the POM-C film (this work T.W.) are shown as a function of kinetic diameter at 30 °C. The continuous fitting line refers to the data set without CO_2, according to eq 16; literature data of other polymers: generic POM,[55] PEO,[58] HDPE,[55,67] PET,[55,68] PFTE,[23] PVF,[23] PVDF,[23] FEP,[24,37] ETFE,[23] PHBVs,[66] and PLA.[70]

The diffusion coefficient exhibited the trend $D_{H_2} > D_{O_2} > D_{CO_2} > D_{N_2}$. Diffusivity, representing the kinetic aspect of mass transport, is generally inversely correlated with the size of the diffusing species and can be expressed by[75]

$$D = A \exp(Bd_k) \tag{15}$$

where A and B are material-specific constants.

As illustrated in Figure 5, the measured diffusivity of CO_2 in POM-C is significantly lower than the value predicted by this relationship. The same behavior is followed by other polymers such as PLA,[70] PHBV,[66,76] and PET,[55,68] whereas PEO seems to not evidence such a deviation.

Concerning the solubility coefficient, the experimental data follow the trend $S_{CO_2} > S_{O_2} > S_{N_2} > S_{H_2}$, which is consistent with the qualitative behavior expected based on gas condensability. More specifically, the critical temperature of the gas (T_C) can be related to the expected solubility coefficients using the following relationship:[77]

$$\ln(S) = CT_C + E \tag{16}$$

where C and E are constants dependent on the material.

As depicted in Figure 6, CO_2 is dissolved in POM-C to a degree that exceeds the predicted correlation, suggesting that the polymer's functional groups may interact with the gas. In summary, the combined analysis of diffusivity and solubility indicates that the trends of CO_2 deviate from those observed for the other gases. The opposing effects of diffusion and solubility do not offset one another; rather, the dominant influence of solubility governs the resulting permeability. These deviations are believed to originate from a common underlying cause, which can be further explored by comparing POM-C with chemically related polymers such as PEO, shedding light on the structural and interaction-based origins of this behavior. POM is chemically related to PEO but contains methylene oxide groups in place of ethylene oxide units. Differences in gas transport between the two polymers can generally be attributed to variations in crystallinity and fractional free volume, which are 0.73 and 0.120 for PEO[58] and 0.5 and 0.086 for POM, respectively. For all gases, these structural factors explain the observed scaling of transport properties between the two polymers (Figures 5 and 6); however, the CO_2 behavior cannot be fully accounted for by crystallinity and free volume alone. This observation further supports strong CO_2–ether oxygen interactions, which are more abundant in POM because it contains a higher density of ether oxygen atoms than in PEO. These interactions, therefore, are expected to enhance CO_2 solubility while prolonging its residence time near the ether groups, thereby reducing its effective diffusivity through the polymer matrix. As a result, the CO_2 solubility in POM-C is roughly three times higher than in PEO, while its diffusivity is more than 20 times lower.[58] This idea is further supported by analogous experimental trends followed by other polymers containing polar groups, such as PLA[70] and PHBV copolymers[66,76] (see Figures 5 and 6). Moreover, molecular dynamics simulations in PHBV[66,76] demonstrated that diffusing CO_2 molecules preferentially localize near carbonyl groups, supporting the expectation that similar local polar interactions occur in POM-C, simultaneously enhancing sorption and reducing diffusion.

4.4. Selective Barrier Performance

The performance of POM-C as a selective gas barrier film is depicted in Figure 7 where the perm-selectivity vs permeability is compared with that of a series of other MAP polymers. Specifically, CO_2/O_2 and O_2/N_2 selectivities are plotted

https://doi.org/10.1021/acsapm.5c03855
ACS Appl. Polym. Mater. 2026, 8, 2619−2631

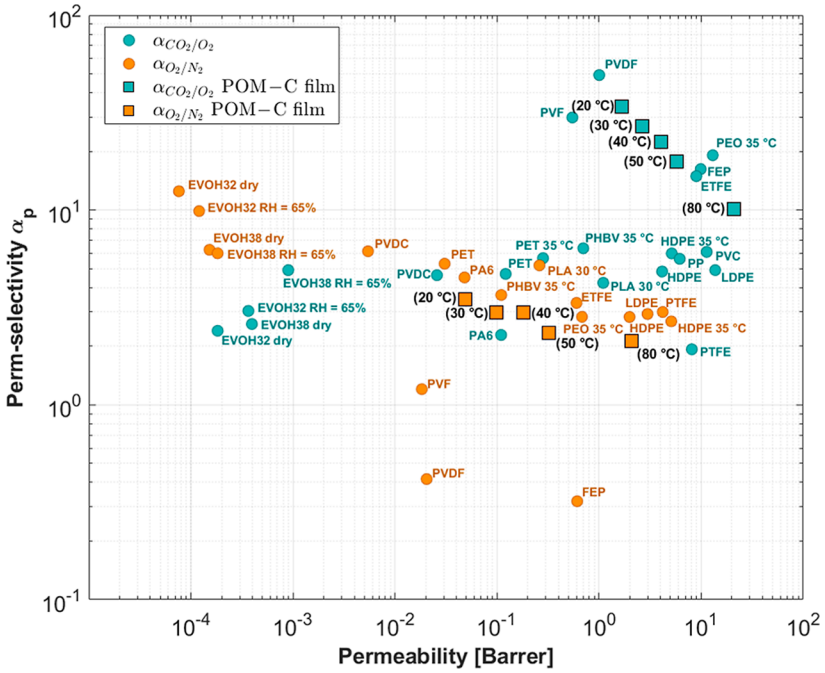

Figure 7. Selective barrier performance landscape: CO_2/O_2 perm-selectivity vs CO_2 permeability (teal) and O_2/N_2 selectivity vs O_2 permeability (orange). Squares represent POM-C film data from this work in the range of 20−80 °C using eq 12. Literature data for other polymers are included: EVOH32,[69] EVOH38,[69] PVDC,[27,37] PET,[27,37] PA6,[27,37] PEO,[58] PP,[27,37] HDPE,[27,37,55] LDPE,[27,37,55] PVC,[27,37] PFTE,[24,37] PVF,[23] PVDF,[24,37] FEP,[23] ETFE,[23] PHBVs,[66] and PLA.[70]

against the permeability of the more permeable gas in each pair—CO_2 and O_2, respectively.

As shown in the chart, POM-C displays a decrease in perm-selectivity and an increase in permeability with rising temperature, consistent with the typical trade-off governing selective transport. The material exhibits O_2/N_2 selectivity values in the range of 2−4, in agreement with the behavior reported for most barrier polymers. At ambient temperature, POM-C performance falls between the values reported for PA6, PHBV, and PET. However, EVOH and PVDC display significantly higher O_2/N_2 selectivity and lower oxygen permeability, indicating superior barrier properties. Conversely, POM-C exhibits a significant CO_2/O_2 selective barrier, similar to fluorinated polymers such as PVF and PVDF. At temperatures of 20 and 30 °C, CO_2/O_2 selectivity reaches values of approximately 34 and 27 respectively, higher than those of PEO, while exhibiting CO_2 permeability roughly 1 order of magnitude lower. This behavior clearly distinguishes it from typical packaging polymers like PP, LDPE, HDPE, and PVC, which generally display both lower selectivity and higher permeability. Compared with PET, PA6, and PVDC, POM-C remains competitive, offering higher selectivity, albeit with a moderately increased permeability. EVOH, however, continues to lead this regime with its combination of good selectivity and extremely low permeability.

Although POM-C's high CO_2/O_2 selectivity (~30) exceeds the optimal range for most conventional MAP applications (typically 3−6), this combination is particularly advantageous for CO_2-sensitive or low- to moderate-respiring commodities—such as mushrooms, asparagus, fresh-cut salads, certain berries, apples, pears, carrots, and nuts—where moderate O_2 influx is sufficient to meet respiration demands, while CO_2 produced by the commodity is vented efficiently.[34,36] By favoring CO_2 permeation relative to O_2, POM-C in this concern may mitigate CO_2 accumulation, off-flavors, and quality degradation during extended storage or long-distance transport, without requiring active gas flushing, which can be particularly valuable for premium or high-value products.[27]

Similar gas management challenges are encountered in bioprocessing containment systems, where structural components or barrier films of the vessel must carefully regulate the gas exchange. Metabolic activity in biofermenters continuously generates CO_2, which must be vented to prevent acidification, pH fluctuations, and growth inhibition.[78] In this context, POM-C presents a material of interest: it maintains moderate CO_2 permeability to allow efficient CO_2 removal, while its high CO_2/O_2 selectivity limits O_2 ingress, helping to mitigate oxidative stress and preserve sensitive metabolic pathways. Likewise, in pharmaceutical packaging, oxygen-sensitive active pharmaceutical ingredients (APIs)—including lyophilized biologics, protein therapeutics, and buffered powders—require effective oxygen exclusion to prevent oxidative degradation.[79−81] POM-C films offer both oxygen and humidity barrier properties while maintaining moderate CO_2 permeability, permitting the diffusion of residual CO_2 from processing or minor reaction byproducts. Given this combination of barrier characteristics, exploring the potential use of POM-C for packaging moisture-sensitive APIs is warranted. Furthermore, strategies such as embedding nanofillers could reduce the permeability without altering the selectivity. In multilayered designs, POM-C could also function as an outer moisture-resistant layer, protecting an inner EVOH core from humidity and thereby preserving its dry-state barrier performance.[82]

5. CONCLUSIONS

A POM-C film (110 μm), produced by hot-melting and compression of a POM-C slab (1 mm), was comprehensively characterized in terms of its permeability, diffusivity, and

https://doi.org/10.1021/acsapm.5c03855
ACS Appl. Polym. Mater. 2026, 8, 2619−2631

solubility. Measurements were conducted using a manometric permeation apparatus at −10−80 °C for CO_2 and H_2 and 20−80 °C for O_2 and N_2. A sample of the pristine slab was also tested between 30 and 50 °C to investigate how variations in thickness, which reflect different processing histories, affect the transport properties. The resulting permeability data follow the trend $P_{CO_2} > P_{H_2} > P_{O_2} > P_{N_2}$ for both the film and the slab, at all temperatures. Despite hydrogen's highest diffusivity due to its small molecular size, the CO_2 permeability is higher due to its markedly greater sorption coefficient, expected to rise from strong interactions between CO_2 molecules and the ether oxygen atoms of the polymer. This enhanced sorption outweighs CO_2's lower diffusivity of CO_2 and governs the overall permeability.

Hydrogen permeability in the film aligns closely with that of the slab, indicating that differences in thickness and the associated processing-induced changes in crystallization and morphology have a negligible impact on hydrogen transport. This result is particularly relevant because it suggests that film data can be representative of thicker materials such as those required in high-pressure storage tanks and pipeline transport. In this context, POM-C displays limited hydrogen permeability (0.44 Barrer at 20 °C), comparable to PA6 (0.24 Barrer at 20 °C), and reaches an exceptionally low value of 0.04 Barrer at −10 °C. Together with its minimal moisture uptake (<0.8%), POM-C represents a promising candidate for hydrogen storage and transport. For the larger gases (CO_2, O_2, and N_2), modest differences between the film and the slab are observed, which generally correlate with crystallinity. The higher crystallinity of the slab increases tortuosity, i.e., the effective diffusion path length around impermeable crystalline regions, resulting in reduced diffusivity and, consequently, lower permeability compared with the film. Such an effect is negligible for hydrogen because its inherently high free-path mobility renders diffusivity largely insensitive to tortuosity, resulting in nearly identical permeability values between the two samples. CO_2 permeability is moderate (1.6 Barrer for the slab at 30 °C), comparable to fluoropolymers such as PVDF, and drops to values as low as 0.215 Barrer at −10 °C. This behavior, together with resistance to corrosive environments and fluorine-free composition, makes it a promising and environmentally friendly candidate for CO_2 storage and transport, including supercritical conditions.

In MAP applications, the POM-C film shows an O_2/N_2 selectivity of around 3−4, in line with common barrier polymers. However, it exhibits markedly higher CO_2/O_2 selectivity (∼30 versus 2−7 for many alternatives) while maintaining CO_2 permeability comparable to HDPE, PP, PLA, PVC, and PTFE. This combination could enable effective CO_2 transport while providing tighter oxygen control, which is particularly valuable for applications such as biofermentation vessels and packaging of moisture-sensitive pharmaceuticals.

Future studies should extend the investigation of transport properties to high-pressure regimes (100−300 bar for CO_2 and up to 700 bar for H_2) to evaluate structural integrity, pressure-induced effects (e.g., blistering), and long-term durability under realistic operating conditions. Such analysis would be essential to assess the practical suitability of POM-C for high-pressure storage and transport applications. Additionally, approaches such as blending POM-C with nanofillers or forming composite systems should be explored to further enhance its barrier performance to meet demanding industrial applications.

■ ASSOCIATED CONTENT

Supporting Information

The Supporting Information is available free of charge at https://pubs.acs.org/doi/10.1021/acsapm.5c03855.

Experimental permeation curves in POM-C (1 mm slab) at 30 °C, 40 °C, and 50 °C for carbon dioxide, hydrogen, oxygen, and nitrogen and linear extrapolation of steady-state behavior (PDF)

■ AUTHOR INFORMATION

Corresponding Author

Omar Atiq − *Department of Civil, Chemical, Environmental, and Materials Engineering, (DICAM), Alma Mater Studiorum—Università di Bologna, 40131 Bologna, Italy;* orcid.org/0000-0002-7528-1367; Email: omar.atiq2@unibo.it

Authors

Lorenzo Merlonghi − *Department of Civil, Chemical, Environmental, and Materials Engineering, (DICAM), Alma Mater Studiorum—Università di Bologna, 40131 Bologna, Italy*

Perla Gavagni − *Department of Civil, Chemical, Environmental, and Materials Engineering, (DICAM), Alma Mater Studiorum—Università di Bologna, 40131 Bologna, Italy*

Marco Giacinti Baschetti − *Department of Civil, Chemical, Environmental, and Materials Engineering, (DICAM), Alma Mater Studiorum—Università di Bologna, 40131 Bologna, Italy;* orcid.org/0000-0002-7327-1608

Complete contact information is available at: https://pubs.acs.org/10.1021/acsapm.5c03855

Notes

The authors declare no competing financial interest.

■ ACKNOWLEDGMENTS

The authors acknowledge the University of Bologna, Department of Civil, Chemical, Environmental and Materials Engineering (DICAM).

■ REFERENCES

(1) Su, Y.; Lv, H.; Zhou, W.; Zhang, C. Review of the Hydrogen Permeability of the Liner Material of Type IV On-Board Hydrogen Storage Tank. *World Elec. Veh. J.* **2021**, *12* (3), 130.

(2) Sun, Y.; Lv, H.; Zhou, W.; Zhang, C. Research on Hydrogen Permeability of Polyamide 6 as the Liner Material for Type IV Hydrogen Storage Tank. *Int. J. Hydrogen Energy* **2020**, *45* (46), 24980−24990.

(3) Sanders, D. F.; Smith, Z. P.; Guo, R.; Robeson, L. M.; McGrath, J. E.; Paul, D. R.; Freeman, B. D. Energy-Efficient Polymeric Gas Separation Membranes for a Sustainable Future: A Review. *Polymer* **2013**, *54* (18), 4729−4761.

(4) Sidhikku Kandath Valappil, R.; Ghasem, N.; Al-Marzouqi, M. Current and Future Trends in Polymer Membrane-Based Gas Separation Technology: A Comprehensive Review. *J. Ind. Eng. Chem.* **2021**, *98*, 103−129.

(5) Lin, J.; Shenogin, S.; Nazarenko, S. Oxygen Solubility and Specific Volume of Rigid Amorphous Fraction in Semicrystalline Poly(Ethylene Terephthalate). *Polymer* **2002**, *43* (17), 4733−4743.
(6) Horas, J. A.; Rizzotto, M. G. Influence of Crystallinity on Gas Transprt in Polymeric Films. *Polym. Eng. Sci.* **1999**, *39* (8), 1389−1393.
(7) Paul, D. R. *Polymeric Gas Separation Membranes*, 1st ed.; CRC Press, 2018.
(8) Doyle, M. J. On the Effect of Crystallinity on the Elastic Properties of Semicrystalline Polyethylene. *Polym. Eng. Sci.* **2000**, *40* (2), 330−335.
(9) Swallowe, G. M. Mechanical Properties and Testing of Polymers. In *Polymer Science and Technology Series*; Brewis, D., Briggs, D., Eds.; Springer Netherlands: Dordrecht, 1999; Vol. 3.
(10) Wu, F.; Misra, M.; Mohanty, A. K. Challenges and New Opportunities on Barrier Performance of Biodegradable Polymers for Sustainable Packaging. *Prog. Polym. Sci.* **2021**, *117*, 101395.
(11) Khalid, H. U.; Ismail, M. C.; Nosbi, N. Permeation Damage of Polymer Liner in Oil and Gas Pipelines: A Review. *Polymers* **2020**, *12* (10), 2307.
(12) Barthelemy, H.; Weber, M.; Barbier, F. Hydrogen Storage: Recent Improvements and Industrial Perspectives. *Int. J. Hydrogen Energy* **2017**, *42* (11), 7254−7262.
(13) Adams, P.; Bengaouer, A.; Cariteau, B.; Molkov, V.; Venetsanos, A. G. Allowable Hydrogen Permeation Rate from Road Vehicles. *Int. J. Hydrogen Energy* **2011**, *36* (3), 2742−2749.
(14) Li, X.; Huang, Q.; Liu, Y.; Zhao, B.; Li, J. Review of the Hydrogen Permeation Test of the Polymer Liner Material of Type IV On-Board Hydrogen Storage Cylinders. *Materials* **2023**, *16* (15), 5366.
(15) Fujiwara, H.; Ono, H.; Ohyama, K.; Kasai, M.; Kaneko, F.; Nishimura, S. Hydrogen Permeation under High Pressure Conditions and the Destruction of Exposed Polyethylene-Property of Polymeric Materials for High-Pressure Hydrogen Devices (2)-. *Int. J. Hydrogen Energy* **2021**, *46* (21), 11832−11848.
(16) Yersak, T. A.; Baker, D. R.; Yanagisawa, Y.; Slavik, S.; Immel, R.; Mack-Gardner, A.; Herrmann, M.; Cai, M. Predictive Model for Depressurization-Induced Blistering of Type IV Tank Liners for Hydrogen Storage. *Int. J. Hydrogen Energy* **2017**, *42* (48), 28910−28917.
(17) Merlonghi, L.; Atiq, O.; Rea, R.; Mangano, E.; Stroeks, A.; Giacinti Baschetti, M.; De Angelis, M. G. An Experimental Study of Hydrogen Sorption and Permeation in High-Performance Polyamides. *Int. J. Hydrogen Energy* **2024**, *88*, 1463−1473.
(18) Zoller, P.; Walsh, D. *Standard Pressure Volume Temperature Data for Polymers*; CRC Press, 1995.
(19) Khanna, Y. P.; Kuhn, W. P. Measurement of Crystalline Index in Nylons by DSC: Complexities and Recommendations. *J. Polym. Sci., Part B: Polym. Phys.* **1997**, *35* (14), 2219−2231.
(20) Parodi, E.; Peters, G. W. M.; Govaert, L. E. Prediction of Plasticity-controlled Failure in Polyamide 6: Influence of Temperature and Relative Humidity. *J. Appl. Polym. Sci.* **2018**, *135* (11), 45942.
(21) Vlasveld, D. P. N.; Groenewold, J.; Bersee, H. E. N.; Picken, S. J. Moisture Absorption in Polyamide-6 Silicate Nanocomposites and Its Influence on the Mechanical Properties. *Polymer* **2005**, *46* (26), 12567−12576.
(22) Arhant, M.; Le Gac, P.-Y.; Le Gall, M.; Burtin, C.; Briançon, C.; Davies, P. Modelling the Non Fickian Water Absorption in Polyamide 6. *Polym. Degrad. Stab.* **2016**, *133*, 404−412.
(23) Tan, Y.; Nookuea, W.; Li, H.; Thorin, E.; Yan, J. Property Impacts on Carbon Capture and Storage (CCS) Processes: A Review. *Energy Convers. Manage.* **2016**, *118*, 204−222.
(24) Signorini, V.; Ansaloni, L.; Peters, T.; Alcock, B.; Giacinti Baschetti, M.; Minelli, M. Characterization and Modeling of CO_2 Transport through Fluorinated Thermoplastics. *ACS Appl. Polym. Mater.* **2024**, *6* (1), 379−389.
(25) Lohmann, R.; Letcher, R. J. The Universe of Fluorinated Polymers and Polymeric Substances and Potential Environmental Impacts and Concerns. *Curr. Opin. Green Sustainable Chem.* **2023**, *41*, 100795.
(26) Tajeddin, B.; Ahmadi, B.; Sohrab, F.; Chenarbon, H. A. Polymers for Modified Atmosphere Packaging Applications. In *Food Packaging and Preservation*; Academic Press, 2018; pp 457−499.
(27) Mangaraj, S.; Goswami, T. K.; Mahajan, P. V. Applications of Plastic Films for Modified Atmosphere Packaging of Fruits and Vegetables: A Review. *Food Eng. Rev.* **2009**, *1* (2), 133−158.
(28) Church, I. J.; Parsons, A. L. Modified Atmosphere Packaging Technology: A Review. *J. Sci. Food Agric.* **1995**, *67* (2), 143−152.
(29) Gorris, L. G. M.; Peppelenbos, H. W. Modified Atmosphere and Vacuum Packaging to Extend the Shelf Life of Respiring Food Products. *HortTechnology* **1992**, *2* (3), 303−309.
(30) Kader, A. A.; Zagory, D.; Kerbel, E. L.; Wang, C. Y. Modified Atmosphere Packaging of Fruits and Vegetables. *Crit. Rev. Food Sci. Nutr.* **1989**, *28* (1), 1−30.
(31) Ohlsson, T.; Bengtsson, N. Minimal Processing Technologies in the Food Industry. In *Woodhead Publishing in food science and technology*; CRC Press: Boca Raton, Fla Cambridge, England, 2002.
(32) Zhuang, H.; Barth, M. M.; Cisneros-Zevallos, L. Modified Atmosphere Packaging for Fresh Fruits and Vegetables. In *Innovations in Food Packaging*; Academic Press, 2014; pp 445−473.
(33) Cooksey, K. Modified Atmosphere Packaging of Meat, Poultry and Fish. In *Innovations in Food Packaging*; Academic Press, 2014; pp 475−493.
(34) Arvanitoyannis, I. *Modified Atmosphere and Active Packaging Technologies*; CRC Press, 2012.
(35) Sivertsvik, M.; Jeksrud, W. K.; Rosnes, J. T. A Review of Modified Atmosphere Packaging of Fish and Fishery Products − Significance of Microbial Growth, Activities and Safety. *Int. J. Food Sci. Technol.* **2002**, *37* (2), 107−127.
(36) Lee, L. Z.; Arul, J.; Castaigne, F.; Lencki, R. Methodology for Determining the Appropriate Selectivity of Mass Transfer Devices for Modified Atmosphere Packaging of Fresh Produce. *Packag. Technol. Sci.* **1996**, *9* (2), 55−72.
(37) Massey, L. K. *Permeability Properties of Plastics and Elastomers, 2nd Ed.: A Guide to Packaging and Barrier Materials*; Cambridge University Press, 2003.
(38) Heinlein, G. S.; Timpe, S. J. Development of Elastic and Plastic Properties of Polyoxymethylene during Bending Fatigue. *J. Appl. Polym. Sci.* **2014**, *131* (18), 40762.
(39) Mohan Babu, K.; Mettilda, M. Studies on Mechanical, Thermal, and Morphological Properties of Glass Fibre Reinforced Polyoxymethylene Nanocomposite. *J. Appl. Chem.* **2014**, *2014*, 1−8.
(40) Bedoui, F.; Fayolle, B. POM Mechanical Properties. In *Polyoxymethylene Handbook*; Lüftl, S., Visakh, P. M., Chandran, S., Eds.; Wiley, 2014; pp 241−255.
(41) Gelbke, H.-P.; Buist, H.; Eisert, R.; Leibold, E.; Sherman, J. H. Derivation of Safe Exposure Levels for Potential Migration of Formaldehyde into Food. *Food Chem. Toxicol.* **2019**, *132*, 110598.
(42) Schuerger, A. C.; Schwendner, P.; Tucker, R. T. Microbial Protocols for Spacecraft: 2. Biocidal Effects of Delrin and Nylon in Sealed Compartments May Enhance Bioburden Reductions in Planetary Spacecraft. *Int. J. Astrobiol.* **2023**, *22* (2), 100−110.
(43) Kongkhlang, T.; Kousaka, Y.; Umemura, T.; Nakaya, D.; Thuamthong, W.; Pattamamongkolchai, Y.; Chirachanchai, S. Role of Primary Amine in Polyoxymethylene (POM)/Bentonite Nanocomposite Formation. *Polymer* **2008**, *49* (6), 1676−1684.
(44) Jiao, Q.; Chen, Q.; Wang, L.; Chen, H.; Li, Y. Investigation on the Crystallization Behaviors of Polyoxymethylene with a Small Amount of Ionic Liquid. *Nanomaterials* **2019**, *9* (2), 206.
(45) Chen, S.; Xu, H.; Duan, H.; Hua, M.; Wei, L.; Shang, H.; Li, J. Influence of Hydrostatic Pressure on Water Absorption of Polyoxymethylene: Experiment and Molecular Dynamics Simulation. *Polym. Adv. Technol.* **2017**, *28* (1), 59−65.
(46) Jiménez, A.; Thompson, G. L.; Matthews, M. A.; Davis, T. A.; Crocker, K.; Lyons, J. S.; Trapotsis, A. Compatibility of Medical-Grade Polymers with Dense CO_2. *J. Supercrit. Fluids* **2007**, *42* (3), 366−372.

https://doi.org/10.1021/acsapm.5c03855
ACS Appl. Polym. Mater. 2026, 8, 2619−2631

(47) Duan, F.; Liu, X.; Qu, D.; Li, B.; Wu, L. Polyoxometalate-Based Ionic Frameworks for Highly Selective CO_2 Capture and Separation. *CCS Chem.* **2021**, *3* (11), 2676−2687.
(48) Yu, B.; Zou, B.; Hu, C.-W. Recent Applications of Polyoxometalates in CO_2 Capture and Transformation. *J. CO2 Util.* **2018**, *26*, 314−322.
(49) Lüftl, S.; Archodoulaki, V.-M.; Seidler, S. Thermal-Oxidative Induced Degradation Behaviour of Polyoxymethylene (POM) Copolymer Detected by TGA/MS. *Polym. Degrad. Stab.* **2006**, *91* (3), 464−471.
(50) Lüftl, S.; Richaud, E. Chemical Resistance of Polyoxymethylene. In *Polyoxymethylene Handbook: Structure, Properties, Applications and Their Nanocomposites*; Lüftl, S., Visakh, P. M., Chandran, S., Eds.; Wiley, 2014; pp 277−299.
(51) Fink, J. K. Physical Properties of Polyoxymethylene. In *Polyoxymethylene Handbook: Structure, Properties, Applications and Their Nanocomposites*; Lüftl, S., Visakh, P. M., Chandran, S., Eds.; Wiley, 2014; pp 227−240.
(52) Wijmans, J. G.; Baker, R. W. The Solution-Diffusion Model: A Review. *J. Membr. Sci.* **1995**, *107* (1−2), 1−21.
(53) Crank, J. *The Mathematics of Diffusion*, 2nd ed.; Oxford University Press: London, 1975.
(54) Leszczynski, P.; Cao, Z.; Wu, H.; Thibault, J.; Kruczek, B. Determination of Time Lag by Accurate Monitoring of Pressure Decay in a New Generation Constant Volume System. *MethodsX* **2024**, *13*, 102858.
(55) Van Krevelen, D. W.; Te Nijenhuis, K. *Properties of Polymers: Their Correlation with Chemical Structure; Their Numerical Estimation and Prediction from Additive Group Contributions*; Elsevier, 2009.
(56) Klopffer, M. H.; Flaconneche, B. Transport Properdines of Gases in Polymers: Bibliographic Review. *Oil Gas Sci. Technol.* **2001**, *56* (3), 223−244.
(57) Härtel, G. Permselectivity of a PA6Membrane for the Separation of a Compressed CO2/H2 Gas Mixture at Elevated Pressures. *J. Membr. Sci.* **1999**, *162* (1−2), 1−8.
(58) Lin, H.; Freeman, B. D. Gas Solubility, Diffusivity and Permeability in Poly(Ethylene Oxide). *J. Membr. Sci.* **2004**, *239* (1), 105−117.
(59) Luo, W.; Hou, D.; Guan, P.; Li, F.; Wang, C.; Li, H.; Zhang, X.; Huang, G.; Lu, X.; Li, Y.; Zhou, T. Pebax Membranes-Based on Different Two-Dimensional Materials for CO2 Capture: A Review. *Sep. Purif. Technol.* **2024**, *340*, 126744.
(60) Minelli, M.; Giacinti Baschetti, M.; Hallinan, D. T.; Balsara, N. P. Study of Gas Permeabilities through Polystyrene-Block-Poly-(Ethylene Oxide) Copolymers. *J. Membr. Sci.* **2013**, *432*, 83−89.
(61) Hughes, S. W. Archimedes Revisited: A Faster, Better, Cheaper Method of Accurately Measuring the Volume of Small Objects. *Phys. Educ.* **2005**, *40* (5), 468−474.
(62) Nedeljkovic, D. The Effect of the Temperature and Moisture to the Permeation Properties of PEO-Based Membranes for Carbon-Dioxide Separation. *Polymers* **2021**, *13* (13), 2053.
(63) Williams, J. L.; Stannett, V. The Diffusion of Gases and Water Vapor through Grafted Polyoxymethylene. *J. Appl. Polym. Sci.* **1970**, *14* (8), 1949−1959.
(64) Galizia, M.; Smith, Z. P.; Sarti, G. C.; Freeman, B. D.; Paul, D. R. Predictive Calculation of Hydrogen and Helium Solubility in Glassy and Rubbery Polymers. *J. Membr. Sci.* **2015**, *475*, 110−121.
(65) Jung, J. K.; Lee, J. H.; Jang, J. S.; Chung, N. K.; Park, C. Y.; Baek, U. B.; Nahm, S. H. Characterization Technique of Gases Permeation Properties in Polymers: H2, He, N2 and Ar Gas. *Sci. Rep.* **2022**, *12* (1), 3328.
(66) Papchenko, K.; Degli Esposti, M.; Minelli, M.; Fabbri, P.; Morselli, D.; De Angelis, M. G. New Sustainable Routes for Gas Separation Membranes: The Properties of Poly(Hydroxybutyrate-Co-Hydroxyvalerate) Cast from Green Solvents. *J. Membr. Sci.* **2022**, *660*, 120847.
(67) Lee, J.-H.; Kim, Y.-W.; Jung, J.-K. Investigation of the Gas Permeation Properties Using the Volumetric Analysis Technique for Polyethylene Materials Enriched with Pure Gases under High Pressure: H2, He, N2, O2 and Ar. *Polymers* **2023**, *15* (19), 4019.
(68) Mercea, P. Permeation of H_2 and D_2 through Polymers. *Isot. Environ. Health Stud.* **1983**, *19* (5), 153−155.
(69) Maes, C.; Luyten, W.; Herremans, G.; Peeters, R.; Carleer, R.; Buntinx, M. Recent Updates on the Barrier Properties of Ethylene Vinyl Alcohol Copolymer (EVOH): A Review. *Polym. Rev.* **2018**, *58* (2), 209−246.
(70) Bao, L.; Dorgan, J. R.; Knauss, D.; Hait, S.; Oliveira, N. S.; Maruccho, I. M. Gas Permeation Properties of Poly(Lactic Acid) Revisited. *J. Membr. Sci.* **2006**, *285* (1−2), 166−172.
(71) Condé-Wolter, J.; Ruf, M. G.; Liebsch, A.; Lebelt, T.; Koch, I.; Drechsler, K.; Gude, M. Hydrogen Permeability of Thermoplastic Composites and Liner Systems for Future Mobility Applications. *Composites, Part A* **2023**, *167*, 107446.
(72) K-Mac Plastics. Acetal Chemical Resistant Chart. http://k-mac-plastics.com/data-sheets/acetal_chemical_resistant_chart.htm. Accessed February 4, 2026.
(73) Foxx Life Sciences. Acetal and Delrin Chemical Compatibility Chart. https://www.foxxlifesciences.com/pages/acetal-chemical-compatibility-chart. Accessed February 4, 2026.
(74) CP Lab Safety. Acetal (Polyoxymethylene) Chemical Compatibility Chart. https://www.calpaclab.com/acetal-polyoxymethylene-chemical-compatibility-chart/?srsltid=AfmBOoqdclD6ed-GEg-MgPHpiCKuoHYnRH5Jb25xBNCcL-BvZj6_sGzc. Accessed February 4, 2026.
(75) Vrentas, J. S.; Duda, J. L. Diffusion in Polymer—Solvent Systems. I. Reexamination of the Free-volume Theory. *J. Polym. Sci., Polym. Phys. Ed.* **1977**, *15* (3), 403−416.
(76) Papchenko, K.; Ricci, E.; De Angelis, M. G. Modelling across Multiple Scales to Design Biopolymer Membranes for Sustainable Gas Separations: 1—Atomistic Approach. *Polymers* **2023**, *15* (7), 1805.
(77) Merkel, T. C.; Bondar, V. I.; Nagai, K.; Freeman, B. D.; Pinnau, I. Gas Sorption, Diffusion, and Permeation in Poly-(Dimethylsiloxane). *J. Polym. Sci., Part B: Polym. Phys.* **2000**, *38* (3), 415−434.
(78) Jurkiewicz, E.; Husemann, U.; Greller, G.; Barbaroux, M.; Fenge, C. Verification of a New Biocompatible Single-Use Film Formulation with Optimized Additive Content for Multiple Bioprocess Applications. *Biotechnol. Prog.* **2014**, *30* (5), 1171−1176.
(79) Lv, Y.; Liu, N.; Chen, C.; Cai, Z.; Li, J. Pharmaceutical Packaging Materials and Medication Safety: A Mini-Review. *Safety* **2025**, *11* (3), 69.
(80) Jaime, S. B. M.; Alves, R. M. V.; Bócoli, P. F. J. Moisture and Oxygen Barrier Properties of Glass, PET and HDPE Bottles for Pharmaceutical Products. *J. Drug Delivery Sci. Technol.* **2022**, *71*, 103330.
(81) Barbaroux, M.; Sette, A. Properties of Materials Used in Single-Use Flexible Containers: Requirements and Analysis. *BioPharm Int.* **2006**, *2006*, 18−29.
(82) Lee, J.; Seo, Y. J.; Kang, D.; Park, C. H.; Shim, J. K. High Strength, High Barrier Polymeric Packaging Film Based on Multi-layered Structure. *J. Appl. Polym. Sci.* **2025**, *142* (17), No. e56788.

https://doi.org/10.1021/acsapm.5c03855
ACS Appl. Polym. Mater. 2026, 8, 2619−2631